Soft x-ray yield from NX2 plasma focus

S. Lee,[1,2,3] R. S. Rawat,[2,a)] P. Lee,[2] and S. H. Saw[1,3]
[1]Institute for Plasma Focus Studies, 32 Oakpark Drive, Chadstone, Victoria 3148, Australia
[2]Natural Sciences and Science Education, National Institute of Education, Nanyang Technological University, Singapore 637616, Singapore
[3]INTI University College, 71800 Nilai, Malaysia

(Received 25 February 2009; accepted 15 June 2009; published online 30 July 2009)

The Lee model code is used to compute neon soft x-ray yield Y_{sxr} for the NX2 plasma focus as a function of pressure. Comparison with measured Y_{sxr} shows reasonable agreement in the Y_{sxr} versus pressure curve, the absolute maximum yield as well as the optimum pressure. This gives confidence that the code gives a good representation of the neon plasma focus in terms of gross properties including speeds and trajectories and soft x-ray yields, despite its lack of modeling localized regions of higher densities and temperatures. Computed current curves versus pressure are presented and discussed particularly in terms of the dynamic resistance of the axial phase. Computed gross properties of the plasma focus including peak discharge current I_{peak}, pinch current I_{pinch}, minimum pinch radius r_{min}, plasma density at the middle duration of pinch n_{pinch}, and plasma temperature at middle duration of pinch T_{pinch} are presented and the trends in variation of these are discussed to explain the peaking of Y_{sxr} at optimum pressure. © *2009 American Institute of Physics*.
[DOI: 10.1063/1.3176489]

I. INTRODUCTION

Plasma focus has been demonstrated as potential x-ray source for various medicobiological and industrial applications such as lithography[1–4] (using ~0.9–1.5 keV photons), radiography,[5,6] microscopy[7,8] (using ~0.25–2.5 keV radiations), and micromachining[9] (using ~4 keV photos). This has led to an increasing interest in exploiting the plasma focus device as a viable intense x-ray source due to some clear advantages such as being relatively cheap, compact, and ease of construction. The x-ray emissions from plasma focus devices have been explored over the wide range of capacitor bank energies ranging from large megajoule and few hundred kilojoule banks[10] to medium sized kilojoule banks[4,11–14] to subkilojoule banks of miniature sized focus devices.[15,16] In the past few years various efforts have been made for enhancing the x-ray yield by changing various experimental parameters such as bank energy,[17] discharge current, electrode configuration (shape and material),[11,13] insulator material and dimensions,[11] gas composition, and filling gas pressure.[5] Thus, soft x-ray yield optimization studies on the plasma focus devices operating over the wide range of bank energies have been one of the actively pursued fields of plasma focus research owing to their vast possible applications. Currently used systematic trial and error experimental procedure to obtain the optimized conditions for maximum radiation yield is highly time-consuming. Hence, the quicker optimization of plasma focus device is highly desirable, which can be achieved if the reliable focus model and corresponding simulation code to predict the x-ray yields from plasma focus device can be developed and used. Obviously the computed yields need to be checked against corresponding measured yields. Further, if the computed soft x-ray yields are consistently reliable against measured values; then it is reasonable to use the computed gross plasma properties as indicative of what we can expect when these plasma properties are measured. In this way, a reliable model code cannot only be used to compute radiation yields, but also be used as a good indicative diagnostic tool for multiple gross plasma properties of the plasma focus.

In the present paper, we used the Lee model code version 13.6b to carry out the numerical experiments on NX2 plasma focus device to compute its neon soft x-ray yield Y_{sxr} as a function of filling gas pressure. The NX2 is a 3 kJ plasma focus originally designed to operate as a neon soft x-ray source with 20 J per shot at 16 shots/s with burst durations of several minutes.[4] Its performance in repetitive mode has been extensively studied, especially in regards to its discharge currents and soft x-ray yield Y_{sxr}. In this paper, we have simulated the operation of NX2 focus device in numerical experiments which are designed to compare its currents, dynamics, and some plasma pinch gross properties at various pressures so as to examine the role played by various relevant plasma properties on the way the Y_{sxr} peaks at the optimum pressure.

II. THE MODEL CODE USED FOR NUMERICAL EXPERIMENTS

The Lee model couples the electrical circuit with plasma focus dynamics, thermodynamics, and radiation, enabling realistic simulation of all gross focus properties. The basic model, described in 1984,[18] was successfully used to assist several projects.[14,19–21] Radiation-coupled dynamics was included in the five-phase code leading to numerical experiments on radiation cooling.[22] The vital role of a finite small disturbance speed discussed by Potter[23] in a *Z*-pinch situation was incorporated together with real gas thermodynamics and radiation-yield terms;[24] this version of the code assisted

[a)]Electronic mail: rajdeep.rawat@nie.edu.sg.

other research projects[4,25,26] and was web-published in 2000[27] and 2005.[28] Plasma self-absorption was included in 2007 (Ref. 27) improving soft x-ray yield simulation. The code has been used extensively in several machines including UNU/ICTP PFF,[4,14,21,25,29] NX2,[4,26] NX1,[4] and adapted for the Filippov-type plasma focus DENA.[30] A recent development is the inclusion of the neutron yield Y_n using a beam-target mechanism,[31–34] incorporated in the present version[35] of the code RADPFV5.13, resulting in realistic Y_n scaling with pinch current I_{pinch}.[31,32] The versatility and utility of the model is demonstrated in its clear distinction of pinch current I_{pinch} from peak discharge current I_{peak} (Ref. 36) and the recent uncovering of a plasma focus pinch current limitation effect[31,33] as well as elucidation of neutron scaling laws to multimega-Joule facilities.[34] The description, theory, code and a broad range of results of this "Universal Plasma Focus Laboratory Facility" is available for download from world wide web.[35]

A brief description, however, of the five phases incorporated in the Lee model code is as follows.

(1) Axial phase: the axial phase is described by a snowplow model with an equation of motion which is coupled to a circuit equation. The equation of motion incorporates the axial phase model parameters: mass and current factors f_m and f_c. The mass swept-up factor f_m accounts for not only the porosity of the current sheath but also for the inclination of the moving current sheath-shock front structure and all other unspecified effects which have effects equivalent to increasing or reducing the amount of mass in the moving structure, during the axial phase. The current factor f_c accounts for the fraction of current effectively flowing in the moving structure (due to all effects such as current shedding at or near the back-wall, current sheet inclination). This defines the fraction of current effectively driving the structure, during the axial phase.

(2) Radial inward shock phase: it is described by four coupled equations using an elongating slug model. The first equation computes the radial inward shock speed from the driving magnetic pressure. The second equation computes the axial elongation speed of the column. The third equation computes the speed of the current sheath, also called the magnetic piston, allowing the current sheath to separate from the shock front by applying an adiabatic approximation. The fourth is the circuit equation. Thermodynamic effects due to ionization and excitation are incorporated into these equations, these effects being important for gases other than hydrogen and deuterium. Temperature and number densities are computed during this phase. A communication delay between shock front and current sheath due to the finite small disturbance speed is crucially implemented in this phase. The model parameters, radial phase mass swept up, and current factors f_{mr} and f_{cr} are incorporated in all three radial phases. The mass swept-up factor f_{mr} accounts for all mechanisms which have effects equivalent to increasing or reducing the amount of mass in the moving slug, during the radial phase not least of which could be axial ejection of mass. The current factor f_{cr} accounts for the fraction of current effectively flowing in the moving piston forming the back of the slug (due to all effects). This defines the fraction of current effectively driving the radial slug.

(3) Radial reflected shock (RS) phase: when the shock front hits the axis, because the focus plasma is collisional, a RS develops which moves radially outwards, while the radial current sheath piston continues to move inwards. Four coupled equations are also used to describe this phase, these being for the RS moving radially outwards, the piston moving radially inwards, the elongation of the annular column and the circuit equation. The same model parameters f_{mr} and f_{cr} are used as in the previous radial phase. The plasma temperature behind the RS undergoes a jump by a factor nearly 2.

(4) Slow compression (quiescent) or pinch phase: when the outgoing RS hits the ingoing piston the compression enters a radiative phase in which for gases such as neon, the radiation emission may actually enhance the compression where we have included energy loss/gain terms from Joule heating and radiation losses into the piston equation of motion. Three coupled equations describe this phase; these being the piston radial motion equation, the pinch column elongation equation and the circuit equation, incorporating the same model parameters as in the previous two phases. Thermodynamic effects are incorporated into this phase. The duration of this slow compression phase is set as the time of transit of small disturbances across the pinched plasma column. The computation of this phase is terminated at the end of this duration.

(5) Expanded column phase: to simulate the current trace beyond this point we allow the column to suddenly attain the radius of the anode, and use the expanded column inductance for further integration. In this final phase the snow plow model is used and two coupled equations are used similar to the axial phase above. This phase is not considered important as it occurs after the focus pinch.

We note that in radial phases 2, 3, and 4, axial acceleration and ejection of mass caused by necking curvatures of the pinching current sheath result in time dependent strongly center-peaked density distributions. Moreover the transition from phase 4 to phase 5 is observed in laboratory measurements to occur in an extremely short time with plasma/current disruptions resulting in localized regions of high densities and temperatures. These center-peaking density effects and localized regions are not modeled in the code, which consequently computes only an average uniform density and an average uniform temperature which are considerably lower than measured peak density and temperature (we thank a Reviewer for his comments regarding this point). However, because the four model parameters are obtained by fitting the computed total current waveform to the measured total current waveform, the model incorporates the energy and mass balances equivalent, at least in the gross sense to all the processes, which are not even specifically modeled. Hence the computed gross features such as speeds and trajectories and integrated soft x-ray yields have been extensively tested in numerical experiments for several machines and are found to be comparable with measured values.

III. X-RAY EMISSIONS IN PLASMA FOCUS AND ITS INCORPORATION IN MODEL CODE

The focused plasma, with electron temperature of a few hundreds of eV to about keV and high enough electron density, is a copious source of x rays. The plasma focus emits both soft (thermal) as well as hard (nonthermal) x rays but for the scope of this paper, we will concentrate only on soft thermal x rays. The plasma focus emits soft thermal x rays by three processes,[37,38] namely: bremsstrahlung (free-free transition) from the Coulomb interactions between electrons and ions; recombination radiation (free-bound transition) emitted by an initially free electron as it loses energy on recombination with an ion; and de-excitation radiation (bound-bound transition) when a bound electron loses energy by falling to a lower ionic energy state. The first two processes give rise to the continuum of the x-ray spectrum, while the third process produces the characteristic line radiation of the plasma. The relative strengths of the continuum and line emissions depend on how the plasma was formed; typically, for a plasma formed from a high-Z material continuum emission dominates, while for a low-Z material line emission can be stronger. The calculation of the power emitted by processes within the plasma depends on assumptions made about the state of the plasma. Following the spectral data obtained by Mahe[24] and Liu *et al.*[25] for the soft x rays from neon operated 3.3 kJ UNU-ICTP plasma focus device, it was found that 64% of soft x-ray emission can be attributed to line radiations at 922 eV (Ly-α) and 1022 eV (He-α) and the remaining 36% by the rest, mainly recombination radiation, for optimized operations. For NX2 plasma focus device, Zhang[39] reported the contribution of line radiation rising to about 80%. It is for these reasons, and also for the temperatures of interest in our numerical experiments on NX2 device we take the neon soft x-ray yield to be equivalent to line radiation yield, i.e., $Y_{\mathrm{sxr}}=Q_L$.

In the code in phase 4, pinch phase neon line radiation Q_L is calculated using the relation

$$\frac{dQ_L}{dt} = -4.6 \times 10^{-31} n_i^2 Z Z_n^4 (\pi r_p^2) z_f / T,$$

after being integrated over the pinch duration. Hence the SXR energy generated within the plasma pinch depends on the properties: number density n_i, effective charge number Z, atomic number of gas Z_n, pinch radius r_p, pinch length z_f, plasma temperature T, and the pinch duration.

This generated energy is then reduced by the plasma self-absorption, which depends primarily on density and temperature; the reduced quantity of energy is then emitted as the SXR yield. It was first pointed by Mahe[24] that a temperature around 300 eV is optimum for SXR production from neon operated plasma. Bing's[26] subsequent work and our subsequent experience through numerical experiments suggest that around 2×10^6 K (below 200 eV) seems to be better. Hence unlike the case of neutron scaling, for neon SXR scaling there is an optimum small range of temperatures (T window) to operate.

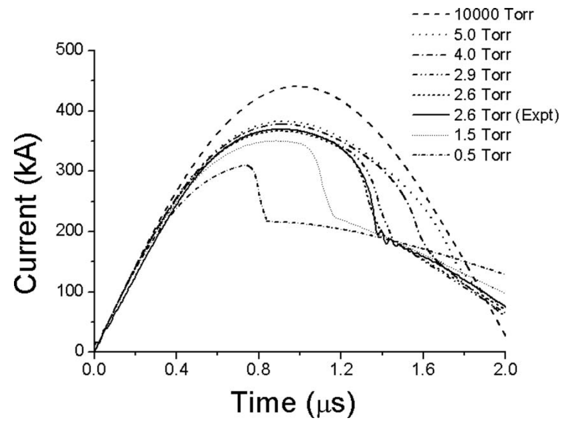

FIG. 1. Fine tuning of Lee model parameter by fitting of computed total current waveform of numerical experiment conducted at 2.6 Torr to that of experimentally measured waveform at same 2.6 Torr of neon. Plots of discharge current waveforms from numerical experiments performed over wide range of neon filling gas pressures are also shown for comparison.

IV. NUMERICAL EXPERIMENTS AND COMPARISON WITH EXPERIMENTAL RESULTS

To start the numerical experiments we select a discharge current trace of the NX2 taken with a Rogowski coil. The selected measured waveform is of a shot at 2.6 Torr neon, near optimum Y_{sxr} yield. The following bank, tube, and operation parameters are used; bank: static inductance $L_0 = 15$ nH, $C_0 = 28$ μF, stray resistance $r_0 = 2.2$ mΩ; tube: cathode radius $b = 4.1$ cm, anode radius $a = 1.9$ cm, anode length $z_0 = 5$ cm; and operation: voltage $V_0 = 11$ kV, pressure $P_0 = 2.6$ Torr.

The computed total current waveform is fitted to the measured waveform by varying model parameters f_m, f_c, f_{mr}, and f_{cr} one by one until the computed waveform agrees with the measured waveform. First, the axial model factors f_m and f_c are adjusted (fitted) until the computed rising slope of the total current trace and the rounding off of the peak current as well as the peak current itself are in reasonable (typically very good) fit with the measured total current trace (see Fig. 1, e.g., 2.6 Torr measured trace and computed trace). Then we proceed to adjust (fit) the radial phase model factors f_{mr} and f_{cr} until the computed slope and depth of the dip agree with the measured. In this case, the following fitted model parameters are obtained: $f_m = 0.1$, $f_c = 0.7$, $f_{\mathrm{mr}} = 0.12$, and $f_{\mathrm{cr}} = 0.68$. These fitted values of the model parameters are then used for the computation of all the discharges at various pressures.

The code is used for each pressure, starting at high pressure (about 10 000 Torr, which is not an issue in numerical experiments although we would not use such pressures in "hardware" experiments) so that the discharge current stayed at the backwall with hardly any motion and hence can be treated as short circuit discharge. The discharge current then resembles that of a simple L-C-R discharge, which is a damped sinusoid. The pressure is then lowered for another

TABLE I. Computed plasma dynamics and pinch plasma parameters for different neon filling gas pressures by numerical experiments conducted on NX2 device using Lee model code. [Parameters used in the table are: I_{peak} is the peak value of the total discharge current; I_{pinch} is the pinch current, taking its value at the start of the pinch phase; peak v_a=peak axial speed, typically end axial speed; S=speed parameter (in kA/cm/Torr$^{1/2}$); peak v_s, v_p=peak radial shock and piston speeds, respectively; r_{min}=minimum radius or focus pinch radius at maximum compression; z_{max}=maximum length of focus pinch at time of maximum compression (note that the anode is hollow); T_{pinch}=plasma temperature at middle of pinch duration; n_i pinch=ion density at the middle of pinch duration; Z=effective charge of the neon plasma at middle of pinch duration; and EINP=work done by the dynamic resistance during radial phase expressed as % of E_0.]

P_0 (Torr)	I_{peak} (kA)	I_{pinch} (kA)	Peak v_a (cm/μs)	S	Peak v_s (cm/μs)	Peak v_p (cm/μs)	r_{min} (cm)	z_{max} (cm)	Pinch duration (ns)	T_{pinch} 10^6 K	n_i pinch (10^{23}/m^3)	Z	EINP (%)	Y_{sxr} (J)
High	440									Middle of pinch				
5	383	76	4.6	90	11.1	8.6	0.86	2.84	100	0.3	1.1	5.5	6.3	0
4.5	381	99	4.8	94	12.2	9.5	0.42	2.7	60	0.47	2.4	7.7	8.6	0
4	378	114	5	99	14.9	11.6	0.29	2.7	46	0.7	3.2	8	10.7	0
3.5	374	128	5.3	105	17	12.8	0.22	2.75	37	1.03	3.9	8	12.9	4.5
3.2	372	135	5.6	109	18.8	13.7	0.19	2.79	34	1.23	4.1	8	14.4	14.6
3	370	140	5.7	113	20	14.1	0.18	2.8	32	1.4	4.1	8	15.2	19.9
2.9	369	142	5.8	114	20.6	14.5	0.17	2.79	30.6	1.51	4	8	15.5	20.8
2.8	369	144	5.9	116	21.1	14.8	0.17	2.79	29.6	1.61	3.8	8	15.7	20
2.7	368	146	6	118	21.8	15	0.18	2.78	28.8	1.72	3.5	8	15.8	17.9
2.6	367	148	6.1	120	22.5	15.3	0.19	2.75	27.3	1.86	3	8	15.8	14.4
2.4	364	152	6.3	124	24.4	15.4	0.22	2.7	23.5	2.18	2.3	8	15.6	8
2	359	159	6.8	134	25.2	16.7	0.25	2.73	23.6	2.8	1.6	8.2	16.2	3.9
1.5	350	164	7.6	151	27.6	18.8	0.26	2.77	22.4	3.9	1.1	8.7	16.7	1.5
1	338	165	8.8	178	32	22.7	0.26	2.77	19.3	5.5	0.7	9.3	16.5	0.4
0.5	310	157	11.1	230	41	28.6	0.26	2.78	15.5	9.4	0.35	10	14.4	0.05

run. This is repeated each time lowering the filling neon pressure. Figure 1 records the discharge current waveforms for some of the selected pressures covering a wide range of neon operating pressures from 5 Torr down to 0.5 Torr. The Fig. 1 also includes the simulated waveform for high pressure shot and measured waveform at 2.6 Torr. It may be noticed that computed total current waveform at 2.6 Torr numerical experiment is almost identical to the measured total current waveform for the 2.6 Torr actual experiment conducted by Zhang indicating an extremely good fine tuning of Lee model parameters, i.e., f_m, f_c, f_{mr}, and f_{cr} [0.1, 0.7, 0.12, and 0.68, respectively, for this shot] and hence provide confidence in simulated results of the gross properties. Figure 1 shows that the unloaded (dynamically) high pressure discharge waveform peaks at about 440 kA just before 1.1 μs. At 5 Torr, the peak of the total current I_{peak} is 380 kA and a small current dip is seen at 1.8 μs which is well after peak current with the total discharge current having dropped to 150 kA at the start of the dip. At successive lower pressure, I_{peak} reduces progressively while the current dip appears at progressively earlier times. At 1.5 Torr, I_{peak} has dropped to 350 kA and the dip starts at about the time of peak current of the high pressure shot. It is reasonable to correlate the current dip with the radial phase, so the shifting of the current dip earlier and earlier at lower and lower pressures is consistent with higher and higher axial speeds. The higher speeds lead to correspondingly higher dynamic resistance (which is numerically half the rate of change of inductance; thus is proportional to the axial speed for an axial run-down tube of constant cross-sectional dimensions). We also tabulate some properties of the dynamics and the pinch plasma as a function of the pressure as computed by numerical experiments. This is shown in Table I.

From the Table I it is seen that optimum Y_{sxr} is computed at P_0=2.9 Torr from the numerical experiments. In order to plot all the properties in one figure each quantity is normalized to its value at optimum, i.e., the value obtained for 2.9 Torr operation. The normalized pinch plasma parameters and absolute Y_{sxr} are then plotted as a function of filling gas pressure of neon (P_0) in Figs. 2(a) and 2(b), respectively. The experimentally measured Y_{sxr} of NX2 operated under similar conditions is also included for comparison. The experimental data in Fig. 2(b) is taken from Fig. 6b of Ref. 4 and also from Fig. 6.7b on page 206 of Ref. 37, and hence the numerical experiments were performed for NX2 device with 5 cm long anode with the device being operated at 11.5 kV. It is evident from Fig. 2(b) (also from Table I) that the Y_{sxr} values from numerical experiments fit the experimentally measured yields reasonably well. It is also necessary to point out here that our computed n_i (being an averaged uniform value) is considerably lower than values measured experimentally. From shock theory we compute for this case (2.6 Torr neon in NX2) a peak on-axis RS value of 2.63 $\times 10^{24}$ ions/m^{-3}. Similarly we compute a peak on-axis RS temperature of 2.7×10^6 K. This illustrates that consideration of density and temperature distributions can allow more realistic estimation of these quantities and even their spatial and temporal distributions. Hence, though our model gives only mean values of the key plasma parameters (such as that of n_i and T) and is unable to trace their evolution with an accuracy that probably can be achieved by modern diagnostics technique, but at the same time we also point out that our average methods allow us to compute realistic gross quantities such as trajectories, speeds, and soft x-ray yields.

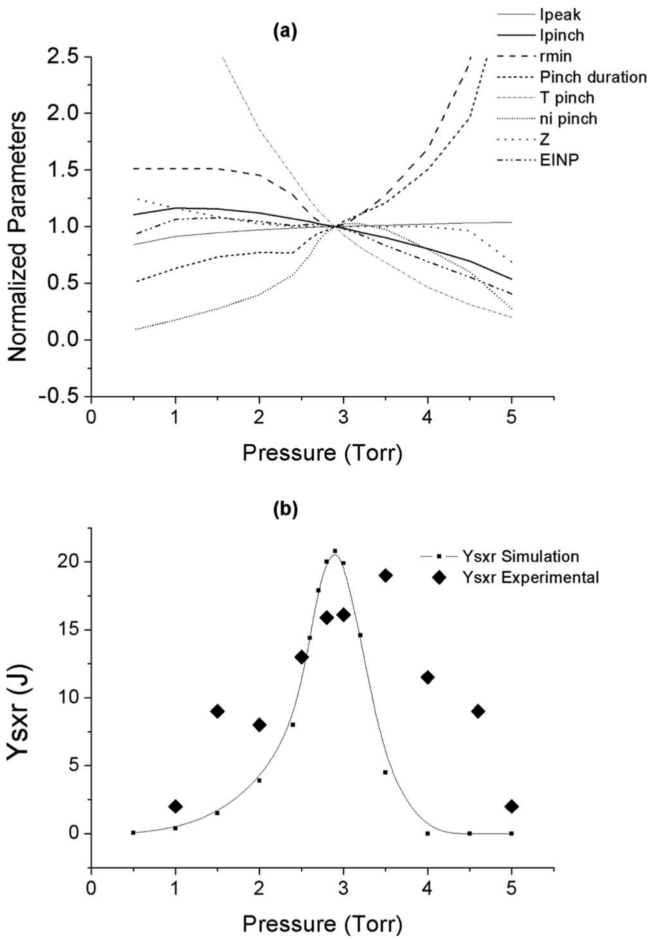

FIG. 2. Effect of operating gas pressure on (a) some key pinch plasma parameters (all normalized using value at optimum operating pressure of 2.9 Torr) and (b) Y_{sxr}; as estimated by numerical experiments. The experimentally measured Y_{sxr} of NX2 operated under similar conditions is also included in (b) for comparison.

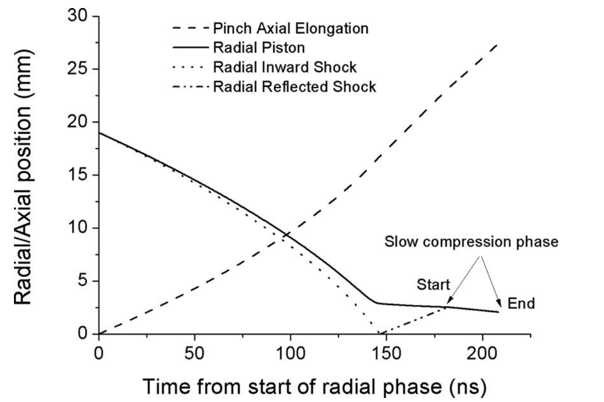

FIG. 3. The currents sheath (radial piston) continues to move in slow compression phase after the radial RS hits it and reaches minimum pinch radius r_{min} at the end of slow compression phase.

V. DISCUSSION OF RESULTS

It is evident from Fig. 2(a) that the peak value of total discharge current I_{peak} decreases with decreasing pressure. This is attributed to increasing dynamic resistance (i.e., increasing rate of change of plasma inductance, dL/dt) due to the increasing current sheath speed as pressure is decreased. We note that, on the contrary, the current I_{pinch} that flows through the pinched plasma column, increases with decreasing pressure. This is due to the shifting of the pinch time toward the time of peak current until the pressure nears 1.2 Torr. As the pressure is decreased below 1.2 Torr, the I_{pinch} starts to decrease as the pinch time now occurs before current peak time. The T_{pinch}, which is the temperature at the middle of the pinch, keeps increasing as pressure is decreased. The n_{pinch}, which is the ion density at middle of the pinch, increases as pressure decreases peaking around 3 Torr and then dropping at lower pressures. The r_{min}, which is the minimum radius of the pinch, has a complementary trend with a minimum at around 3 Torr. This shows that as the operating pressure is reduced toward 3 Torr, the increasing I_{pinch} increases the compression sufficiently so that despite the drop in ambient number density, the pinch n_i is still able to reach a higher value at 3 Torr. As the operating pressure is reduced below 3 Torr, the increase in I_{pinch} does not appear to be sufficient to further increase n_i or indeed even to compress the pinch to a smaller radius than at 3 Torr. To clarify this situation we briefly explain the plasma dynamics during the radial collapse phase.

The radial phase uses a slug model with an imploding cylindrical shock wave forming the front of the slug, driven by a cylindrical magnetically driven current sheath piston at the rear of the slug. Between the shock wave and the current sheath is the shock heated plasma. When the shock front implodes onto the tube axis, because the plasma is collisional, a RS develops. The RS front moves radially outwards into the inwardly streaming particles of the plasma slug, leaving behind it a stationary doubly shocked plasma with a higher temperature and density than the singly shocked plasma ahead of it. When the RS reaches the incoming current sheath, typically the magnetic pressure exceeds the doubly shocked plasma pressure, in which case the current sheath continues inwards in a further slow compression, until the end of this quasiequilibrium phase. The duration of this slow compression phase may be defined by the transit time of small disturbances. For a well-designed and operated plasma focus there is a slow compression throughout this whole duration and the pinch radius reaches its minimum r_{min} at the end of the phase. These various phases/phenomena can be seen in Fig. 3. The radiation yield depends on: (a) the absolute density (which depends on the ambient density and the compression of which r_{min} is a measure, the smaller r_{min}/a where a is the anode radius, the greater the compression), (b) the temperature (which depends on the imploding speeds [the lower the operating pressure, the higher the imploding speeds, noting that shocked temperatures depends on the square of the shock speeds] and the further compression), (c) the duration of the slow compression phase (which scales inversely as the square root of the pinch temperature), and (d) the volume of the pinched plasma during the slow compression phase (which predominantly scales as a). Thus, in this particular example, as the operating pressure is reduced below 3 Torr, although I_{pinch} still increases, speeds also increase, increasing the temperature, which tends to oppose the severity of the compression during the slow compression phase, although the decreased ambient number density tends to work in the opposite direction. The interaction of all these factors are taken care of in the code and manifests in the peaking of n_i at 3.1 Torr and the minimum value of $r_{\min}$ at 2.9 Torr. Moreover, as can be seen in Table I, the pinch duration progressively reduces, as the temperature increases with lowering pressure; while the radiating plasma volume reaches a minimum around 2.9 Torr. The interactions of all the behavior of $r_{\min}$, n_i, and T_{pinch}, pinch duration and plasma volume all contribute to the peak in Y_{sxr} as a function of operating pressure. Looking at the Table I and Fig. 2(a) it does appear that the peaking of n_{pinch} at 3.1 Torr is a notable factor for the peaking of Y_{sxr} at 2.9 Torr.

The Fig. 2(b) shows reasonable agreement the results of numerical experiments and experimentally measured; in terms of absolute value of Y_{sxr} at optimum pressure (about 20.8 J by numerical experiment, refer Table I, and about 16.1 J as experimentally measured[4,39]) as well as the optimum pressure value itself. The computed curve falls off more sharply on both sides of the optimum pressure. This agreement validates our views that the fitting of the computed total current waveform with the measured waveform enables the model to be energetically correct in all the gross properties of the radial dynamics including speeds and trajectories and soft x-ray yields despite the lack of fine features in the modeling.

VI. CONCLUSIONS

To conclude, the Lee model code has been successfully used to perform numerical experiments to compute neon soft x-ray yield for the NX2 as a function of pressure with reasonable degree of agreement in (i) the Y_{sxr} versus pressure curve trends, (ii) the absolute maximum yield, and (iii) the optimum pressure value. The only input required is a measured total current waveform. This reasonably good agreement, against the background of an extremely complicated situation to model, moreover the difficulties in measuring Y_{sxr}, gives confidence that the model is sufficiently realistic in describing the plasma focus dynamics and soft x-ray emission for NX2 operating in Neon. This encourages us to present Table I and to present the above views regarding the factors contributing to the peaking of Y_{sxr} at an optimum pressure.

[1] D. Wong, A. Patran, T. L. Tan, R. S. Rawat, and P. Lee, IEEE Trans. Plasma Sci. **32**, 2227 (2004).
[2] R. Petr, A. Bykanov, J. Freshman, D. Reilly, J. Mangano, M. Roche, J. Dickenson, M. Burte, and J. Heaton, Rev. Sci. Instrum. **75**, 2551 (2004).
[3] Y. Kato, I. Ochiai, Y. Watanabe, and S. Murayama, J. Vac. Sci. Technol. B **6**, 195 (1988).
[4] S. Lee, P. Lee, G. Zhang, X. Feng, V. A. Gribkov, M. Liu, A. Serban, and T. K. S. Wong, IEEE Trans. Plasma Sci. **26**, 1119 (1998).
[5] F. N. Beg, I. Ross, A. Lorena, J. F. Worley, A. E. Dangor, and M. G. Hanies, J. Appl. Phys. **88**, 3225 (2000).
[6] S. Hussain, M. Shafiq, R. Ahmad, A. Waheed, and M. Zakaullah, Plasma Sources Sci. Technol. **14**, 61 (2005).
[7] F. Castillo-Mejia, M. M. Milanese, R. L. Moroso, J. O. Pouzo, and M. A. Santiago, IEEE Trans. Plasma Sci. **29**, 921 (2001).
[8] R. S. Rawat, T. Zhang, G. J. Lim, W. H. Tan, S. J. Ng, A. Patran, S. M. Hassan, S. V. Springham, T. L. Tan, M. Zakaullah, S. Lee, and P. Lee, J. Fusion Energy **23**, 49 (2004).
[9] V. A. Gribkov, A. Srivastava, P. L. C. Keat, V. Kudryashov, and S. Lee, IEEE Trans. Plasma Sci. **30**, 1331 (2002).
[10] V. A. Gribkov, B. Bienkowska, M. Borowiecki, A. V. Dubrovsky, I. Ivanova-Stanik, L. Karpinski, R. A. Miklaszewski, M. Paduch, M. Scholz, and K. Tomaszewski, J. Phys. D **40**, 1977 (2007).
[11] M. Zakullah, K. Alamgir, M. Shafiq, S. M. Hassan, M. Sharif, S. Hussain, and A. Waheed, Plasma Sources Sci. Technol. **11**, 377 (2002).
[12] R. S. Rawat, T. Zhang, C. B. L. Phua, J. X. Y. Then, K. A. Chandra, X. Lin, A. Patran, and P. Lee, Plasma Sources Sci. Technol. **13**, 569 (2004).
[13] H. Bhuyan, S. R. Mohanty, N. K. Neog, S. Bujarbarua, and R. K. Rout, J. Appl. Phys. **95**, 2975 (2004).
[14] S. Lee, T. Y. Tou, S. P. Moo, M. A. Eissa, A. V. Gholap, K. H. Kwek, S. Mulyodrono, A. J. Smith, Suryadi, W. Usada, and M. Zakaullah, Am. J. Phys. **56**, 62 (1988).
[15] R. Verma, P. Lee, S. V. Springham, T. L. Tan, M. Krishnan, and R. S. Rawat, Appl. Phys. Lett. **92**, 011506 (2008).
[16] P. Silva, J. Moreno, C. Pavez, L. Soto, and J. Arancibia, J. Phys.: Conf. Ser. **134**, 012044 (2008).
[17] P. G. Burkhalter, G. Mehlman, D. A. Newman, M. Krishnan, and R. R. Prasad, Rev. Sci. Instrum. **63**, 5052 (1992).
[18] S. Lee, in *Radiations in Plasmas*, edited by B. McNamara (World Scientific, Singapore, 1984), p. 978.
[19] T. Y. Tou, S. Lee, and K. H. Kwek, IEEE Trans. Plasma Sci. **17**, 311 (1989).
[20] S. Lee, IEEE Trans. Plasma Sci. **19**, 912 (1991).
[21] A. Serban and S. Lee, J. Plasma Phys. **60**, 3 (1998).
[22] J. b. Ali, "Development and studies of a small plasma focus," Ph.D. thesis, Universiti Teknologi Malaysia, 1990.
[23] D. E. Potter, Nucl. Fusion **18**, 813 (1978).
[24] L. Mahe, "Soft x-rays from compact plasma focus," Ph.D. thesis, Nanyang Technological University, 1996.
[25] M. Liu, X. P. Feng, S. V. Springham, and S. Lee, IEEE Trans. Plasma Sci. **26**, 135 (1998).
[26] S. Bing, "Plasma dynamics and x-ray emission of the plasma focus," Ph.D. thesis, Nanyang Technological University, 2000; ICTP Open Access Archive: http://eprints.ictp.it/99/.
[27] S. Lee, http://ckplee.myplace.nie.edu.sg/plasmaphysics/, 2000.
[28] S. Lee, ICTP Open Access Archive: http://eprints.ictp.it/85/13, 2005.
[29] S. Lee, Twelve Years of UNU/ICTP PFF—A Review IC 98 (231), Miramare, Trieste, 1998 (unpublished).
[30] V. Siahpoush, M. A. Tafreshi, S. Sobhanian, and S. Khorram, Plasma Phys. Controlled Fusion **47**, 1065 (2005).
[31] S. Lee and S. H. Saw, Appl. Phys. Lett. **92**, 021503 (2008).
[32] S. Lee and S. H. Saw, J. Fusion Energy **27**, 292 (2008).
[33] S. Lee, P. Lee, S. H. Saw, and R. S. Rawat, Plasma Phys. Controlled Fusion **50**, 065012 (2008).
[34] S. Lee, Plasma Phys. Controlled Fusion **50**, 105005 (2008).
[35] S. Lee, Radiative Dense Plasma Focus Computation Package: RADPF http://www.intimal.edu.my/school/fas/UFLF/.
[36] S. Lee, S. H. Saw, P. C. K. Lee, R. S. Rawat, and H. Schmidt, Appl. Phys. Lett. **92**, 111501 (2008).
[37] E. H. Beckner, J. Appl. Phys. **37**, 4944 (1966).
[38] W. H. Bostic, V. Nardi, and W. Prior, J. Plasma Phys. **8**, 1 (1972).
[39] Z. Guixin, "Plasma soft x-ray source for microelectronic lithography," Ph.D. thesis, Nanyang Technological University, 1999.